Available online at www.sciencedirect.com
SCIENCE DIRECT®
PERGAMON
International Journal of Heat and Mass Transfer 46 (2003) 2193–2205
International Journal of HEAT and MASS TRANSFER
www.elsevier.com/locate/ijhmt

Two-dimensional model of heat transfer in circulating fluidized beds. Part II: Heat transfer in a high density CFB and sensitivity analysis

D. Xie, B.D. Bowen, J.R. Grace *, C.J. Lim

Department of Chemical and Biological Engineering, University of British Columbia, 2216 Main Mall, Vancouver, Canada V6T 1Z4

Received 10 May 2002; received in revised form 20 September 2002

Abstract

Experiments were conducted in a 76 mm diameter jacketed riser of a dual-loop high-density circulating fluidized bed facility with FCC particles of 65 μm Sauter mean diameter as bed material. The suspension temperature and the average and local suspension-to-wall heat transfer coefficients were measured. After superimposing the heat transfer results when the suspension near the wall is allowed to move intermittently downwards and upwards, the model proposed in Part I predicts the experimental results well. The model is used to investigate the effects of various operating parameters on the heat transfer process.

1. Introduction

Circulating fluidized bed risers have been investigated extensively for the past two decades because of their practical applications, as well as their intrinsic interest. However, the overwhelming majority of such work has been conducted at net solids fluxes, G_s, less than 100 kg/m^2 s, and at superficial gas velocities, U_g, between about 2 and 8 m/s. For these conditions, the overall volumetric solids concentrations, c, is less than about 0.1 [1]. While these conditions are relevant to circulating fluidized bed (CFB) combustion, much higher solids fluxes and holdups are encountered in CFB risers used for solid catalyzed reactions like fluid catalytic cracking and production of maleic anhydride. In such cases, G_s is commonly 300–1200 kg/m^2 s, with corresponding c values ranging from 0.07 to 0.25. Grace et al. [2] defined the dense suspension upflow regime as having $G_s > 200$ kg/m^2 s, $c > 0.07$ and solids upflow on average throughout the entire riser. Published results demonstrate that such operations differ in several important respects from low-density circulating fluidized bed systems.

While numerous experiments have been carried out to investigate heat transfer in circulating fluidized beds, almost none of these applies to the high-density conditions defined above. CFB bed-to-wall heat transfer is strongly influenced by the flow pattern in the riser, especially the particle motion in the vicinity of the wall. Experimental work is needed to elucidate the heat transfer behavior in the high-density flow regime and to modify the model which was developed in Part I for low-density operating conditions.

2. Experimental facilities

2.1. High-density circulating fluidized bed system

The dual-loop high-density circulating fluidized bed (HDCFB) system located at the University of British Columbia consists of two Plexiglas risers, two PVC downcomers, a curved plate impingment separator, cyclones and an air filter baghouse. The first riser has a diameter of 76.2 mm and a height of 6.10 m, while the second riser has a diameter of 101.6 mm and height of

* Corresponding author. Tel.: +1-604-822-3121/3238; fax: +1-604-822-6003.
E-mail address: jgrace@chml.ubc.ca (J.R. Grace).

0017-9310/03/$ - see front matter © 2003 Elsevier Science Ltd. All rights reserved.
doi:10.1016/S0017-9310(02)00528-8

Nomenclature

A_c	total inside area of the inner cylinder
C	volume fraction occupied by solids
C_{pc}	cooling water heat capacity
d_p	particle diameter
f_d	time-averaged fraction of particles moving downward in the vicinity of wall
G_s	solid circulation flux
g	acceleration due to gravity
h	bed-to-wall heat transfer coefficient
h'	bed-to-water-side wall heat transfer coefficient
h_d	bed-to-wall heat transfer coefficient due to downward particle motion in the vicinity of wall
h_u	bed-to-wall heat transfer coefficient due to upward particle motion in the vicinity of wall
L_{ar}	particle average residence length in wall layer
L_w	wall thickness
m_c	cooling water flowrate
r	radius
R	inner radius of inner tube of concentric heat exchanger
r_1	outer radius of inner tube of concentric heat exchanger
r_2	inner radius of outer tube of concentric heat exchanger
T_b	bulk temperature
T_c	cross-sectional average coolant temperature
$T_{c,in}$	T_c at inlet of heat exchanger or at inlet of each section
$T_{c,out}$	T_c at outlet of heat exchanger or at outlet of each section
T_{sbc}	suspension temperature at center of riser below heat exchanger
T_{sbw}	suspension temperature near wall below heat exchanger
T_{stc}	suspension temperature at center of riser above heat exchanger
T_{stw}	suspension temperature near wall above heat exchanger
$T_{w,in}$	T_w at inlet of heat exchanger or at inlet of each section
$T_{w,out}$	T_w at outlet of heat exchanger or at outlet of each section
U_g	superficial gas velocity
U_{mf}	particle minimum fluidization velocity
x	dimensionless radial coordinate, r/R
z	vertical coordinate, directed vertically downward
Z	height above air distributor

Greek symbols

ε_{mf}	loosely packed bed voidage
ρ_{sus}	suspension density
ΔP	pressure difference
ΔZ	distance between differential pressure ports

9.14 m. Other details of this system are provided by Xie [3].

2.2. Heat transfer measurement equipment

The heat transfer system consisted of a concentric-tube heat exchanger, a steam-water heat exchanger, a steam trap, four needle valves and a rotameter. The concentric-tube heat exchanger, shown in Fig. 1, replaced one of the Plexiglas sections near the center of the 76.2 mm diameter riser. Four K-type thermocouples were mounted on the outside surface of the inner tube to measure the wall surface temperatures. Four ports were provided on the outer tube where temperature probes can be inserted into the water flowing through the annular jacket. Water entered the bottom of the exchanger through four inlets, uniformly distributed at 90° intervals. It left the exchanger from the top, again through four evenly distributed ports. The entire riser including the heat exchange section as well as the water inlet and outlet tubes were wrapped in fiberglass insulation, with the heat exchanger being especially well insulated.

2.3. Bed material

FCC particles of Sauter mean diameter 65 μm and density 1600 kg/m^3 were used in all experiments. Their minimum fluidization velocity, U_{mf}, was 0.0032 m/s in air at atmospheric temperature and pressure. The loose packed bed voidage, ε_{mf}, was 0.45.

2.4. Measurement techniques

Superficial gas velocities were measured in both risers using orifice meters. The solids circulation flux was measured by a butterfly valve installed in the upper part of the downcomer. During measurements, the two halves were rapidly rotated upward to the horizontal position, thus trapping the downflowing solids. The solids circulation rate was calculated from the time

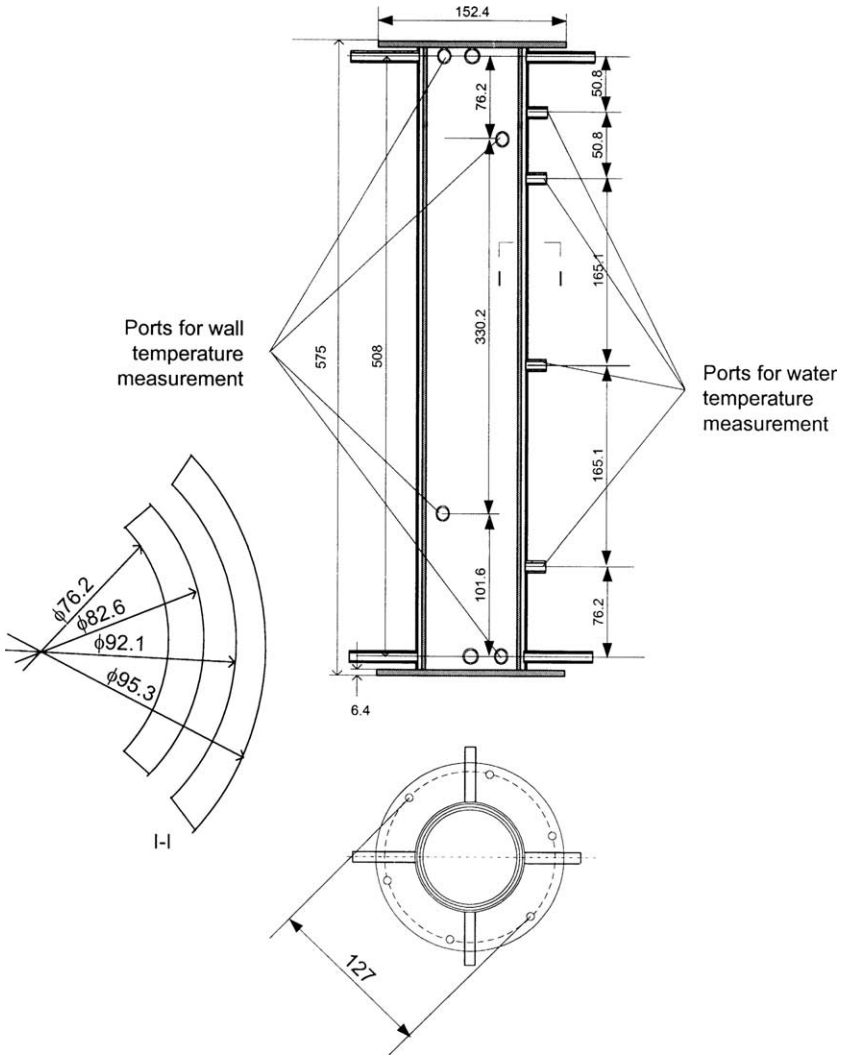

Fig. 1. Concentric-tube heat exchanger. All dimensions in millimeters.

needed to accumulate a known volume of solids on top of the valve. The cross-sectional area-averaged suspension density is estimated from the pressure gradient. If solids acceleration and the effects of gas-wall and solid-wall friction are neglected, the average suspension density is given by

$$\rho_{\text{sus}} = -\frac{1}{g}\frac{\Delta P}{\Delta Z}. \quad (1)$$

The riser was equipped with 7.9 mm diameter ports through which thermocouples can be inserted and moved in and out to measure the suspension temperature at different axial and radial positions.

Using steam, the water was preheated to about 85 °C to provide a sufficient driving force for heat transfer to the bed suspension. To maintain an accurately measurable difference between the water inlet and outlet temperatures, the water flowrate had to be kept very low, usually 30 ml/s, which led to laminar flow in the annular channel between the two tubes. Hence the radial temperature distribution had to be measured in order for the bulk-average water temperature to be calculated.

Four probes of the type shown in Fig. 2 were specially constructed to measure the radial water temperature distribution in the annular channel. Each probe consisted of an acrylic shell and four pairs of 0.38 mm OD. K-type thermocouple wires. Each pair of wires passing through the inside of the tube was joined to form a thermocouple junction at the circumferential surface of the shell, and the distance from each junction to the probe tip was precisely determined. When installed, each probe was inserted until it made contact with the inner tube of the heat exchanger, where it was locked in place.

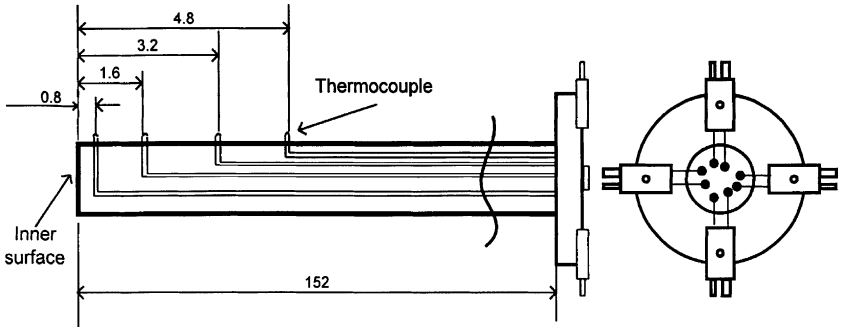

Fig. 2. Set-up for water temperature measurements. All dimensions in millimeters.

Based on the laminar velocity profile of the water in the annular channel and the radial temperature profile measured by each probe, the bulk-average water temperature could be determined at the four probe locations (see Xie [3] for details). The water inlet and outlet temperatures were also measured using standard Omega KQIN-18U thermocouples.

For each measurement, at least 30 min were required until the column reached steady state. The sampling frequency of the data acquisition system was 1 Hz. All steady state temperatures were obtained by averaging instantaneous measurements over 5 min. Typical standard deviations were 0.5 °C for suspension temperatures and 0.1 °C for water and wall temperature measurements.

3. Experimental results and discussion

3.1. Suspension temperature distribution

The suspension temperatures were recorded above and below the heat exchange section, 3.85, 3.25, 2.35, 2.05, 1.45, 1.15 and 0.84 m above the gas distributor. Fig. 3 shows the vertical and radial suspension temperature distributions for three different operating conditions at $U_g = 6$ m/s. To simplify the following discussion, the suspension temperature at a specific location is denoted by $T_s(x, Z)$, where $x = r/R$ represents the dimensionless radial coordinate and Z is the height above the distributor. For condition A, the radial temperature profiles are quite flat at all levels except $Z = 3.25$ m, which is immediately above the water jacket. At this vertical position, the suspension temperature at the wall is significantly higher than at the center. The difference between $T_s(1, 2.35)$ and $T_s(0, 2.35)$ (just below the heat exchanger section) is much smaller than that between $T_s(1, 3.25)$ and $T_s(0, 3.25)$. Also $T_s(1, 2.35)$ is greater than $T_s(1, 2.05)$, while $T_s(1, 3.25)$ is greater than $T_s(1, 3.85)$. Since the heat exchanger extends from $Z = 2.50$ to 3.10 m, these trends imply that the particles in the vicinity of wall were mostly traveling upwards, while spending a small fraction of time descending, or perhaps oscillating back and forth close to the wall.

For operating condition B, it can be seen that $T_s(1, 2.35) > T_s(1, 3.25)$, and, contrary to run A, $[T_s(1, 2.35) - T_s(0, 2.35)]$ is greater than $[T_s(1, 3.25) - T_s(0, 3.25)]$. This indicates that for this condition most particles near the wall were descending, causing the temperature below the water jacket to be higher than that above. On the other hand, $T_s(1, 3.25)$ remains higher than $T_s(1, 3.85)$, suggesting that there may also have been some rising particles in the wall region.

In run C with $G_s = 26$ kg/m^2 s and $\rho_{sus} = 19$ kg/m^3, $T_s(1, 2.35)$ and $T_s(1, 3.25)$ are almost the same, while $[T_s(1, 2.35) - T_s(0, 2.35)]$ is a little greater than $[T_s(1, 3.25) - T_s(0, 3.25)]$. This indicates that while the majority of the particles in the vicinity of wall were descending, a significant fraction may have been ascending.

Issangya [4] reported suspension density profiles and measured local solids mass fluxes in the same column using sampling probes at $r/R = 0.95$ and $Z = 2.8$ m, corresponding to the center of our heat exchanger for conditions similar to those covered in the heat transfer experiments of this paper. In all his tests, particles were always observed to move both upward and downward in the vicinity of wall. In the fast fluidization flow regime, most particles were observed to descend, but when the net circulation flux increased, the majority of particles rose near the wall. Liu [5] measured local particle velocities using a multifunctional probe in the same column for similar particles and operating conditions. He found that when $G_s > 500$ kg/m^2 s, particles traveled upward on a time-mean basis across the entire riser cross-section.

From these observations, one can construct a likely picture of particle motion in the vicinity of wall. In the pneumatic conveying regime, when there are very few particles in the suspension, particles all move upwards in the riser. As G_s increases, more particles accumulate in the column, and those close to the wall begin to descend. When the net solids flux in the vicinity of the wall is

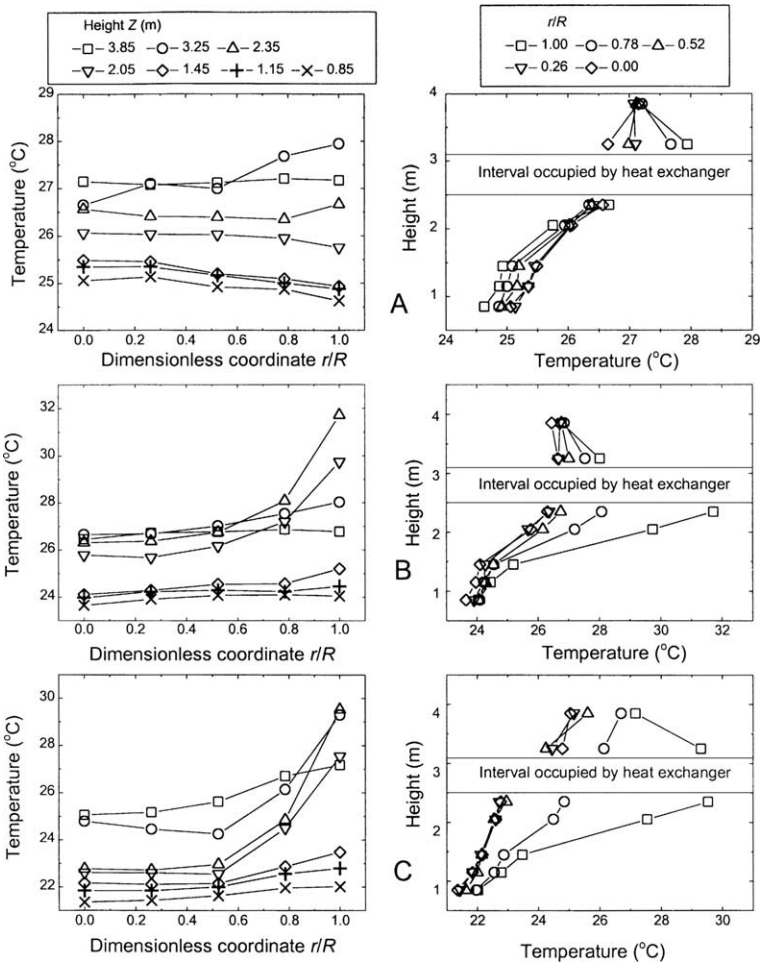

Fig. 3. Radial and vertical bed temperature distribution for $U_g = 6$ m/s. A: $G_s = 282$ kg/m^2 s, $\rho_{sus} = 342$ kg/m^3; B: $G_s = 213$ kg/m^2 s, $\rho_{sus} = 136$ kg/m^3; C: $G_s = 26$ kg/m^2 s, $\rho_{sus} = 19$ kg/m^3.

downwards, a wall layer forms and the fast fluidization flow regime is reached. However, if G_s continues to increase, the suspension becomes denser, with more particles in the wall layer carried up until the net solids flux in the vicinity of the wall again becomes upwards and the annular downflowing wall layer is eliminated. The system is then operating as a dense suspension upflow. For G_s extremely high, >500 kg/m^2 s for our experimental set-up, few particles descend in the vicinity of the wall.

3.2. Average heat transfer coefficient

For steady-state conditions with losses from the outside of the jacket ignored, energy conservation requires that the total heat supplied by the hot water equals the heat transferred from the water to the suspension. Since the water-side wall surface temperature is measured, the suspension-to-wall-surface heat transfer coefficient can be calculated from

$$h' = \frac{m_c C_{pc}(T_{c,in} - T_{c,out})}{A_c \Delta T_{sus\text{-}to\text{-}wall}}, \tag{2}$$

where

$$\Delta T_{sus\text{-}to\text{-}wall} = \frac{(T_{w,in} - T_{sbc}) - (T_{w,out} - T_{stc})}{\ln((T_{w,in} - T_{sbc})/(T_{w,out} - T_{stc}))}. \tag{3}$$

The total thermal resistance from the suspension to the water-side wall surface is the sum of the thermal resistance on the suspension side and that due to conduction in the tube wall. Hence the suspension-to-wall heat transfer coefficient is

$$h = \frac{1}{(1/h') - (r_1 \ln(r_1/R)/k_w)}. \tag{4}$$

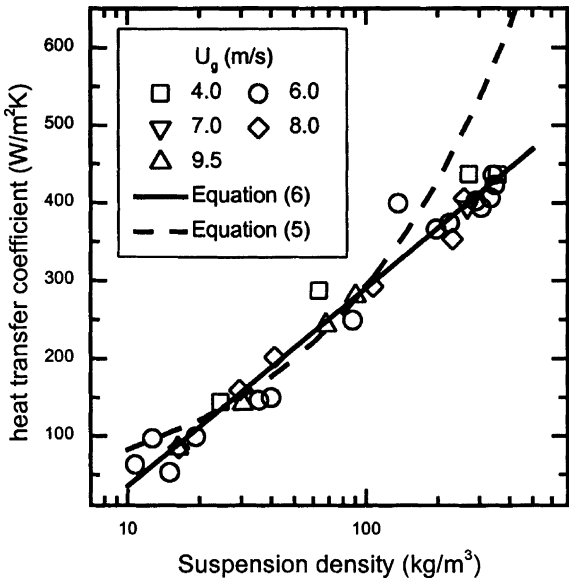

Fig. 4. Suspension-to-wall heat transfer coefficient vs. suspension density.

It has been widely reported that, at constant suspension density, the superficial gas velocity does not have a significant influence on the heat transfer coefficient [6,7]. Fig. 4 shows the suspension-to-wall heat transfer coefficient as a function of suspension density and superficial gas velocity. It can be seen that, for a given suspension density, the heat transfer coefficient is hardly influenced by the superficial gas velocity, as in the previous studies.

Divillo and Boyd [8] correlated the convective suspension-to-wall heat transfer coefficient as a function of suspension density based on data from different cold units and obtained:

$$h = 23.2\rho_{\mathrm{sus}}^{0.55}. \tag{5}$$

This relationship, plotted as a dashed line in Fig. 4, overestimates our heat transfer coefficient data for $\rho_{\mathrm{sus}} > 200$ kg/m^3. Our experimental data are better correlated by the following logarithmic relationship, shown as a solid line in Fig. 4:

$$h = 111 \ln \rho_{\mathrm{sus}} - 221 \quad (10 < \rho_{\mathrm{sus}} < 400 \text{ kg/m}^3). \tag{6}$$

3.3. Local heat transfer coefficient

As described above, probes containing four thermocouples each were inserted into the annular water channel at four levels, while two regular thermocouples measured the bulk temperatures at the water inlet and outlet. The water jacket is therefore divided into five sections in series bounded by these six measurement levels. For each section, the average heat transfer coefficient is calculated from Eqs. (2)–(4), with the wall surface temperatures at the ends of each section calculated from cubic splines fitted to the four wall surface temperature measurements.

The experimental results are illustrated in Figs. 5 and 6 as solid points for superficial gas velocities of 6 and 8 m/s, respectively. The operating conditions are listed in Table 1. For both gas velocities, the heat transfer coefficients pass through a minimum between the top and bottom of the water jacket, except for conditions A and F, corresponding to the highest net particle circulation flux, where the heat transfer coefficient decreases with height along the entire length of the jacketed section.

As discussed above, the behavior of the suspension-to-wall heat transfer coefficient is closely associated with the particle motion in the vicinity of the wall, and the direction of this motion is indicated by the suspension temperature distribution. The suspension temperatures in the vicinity of the wall and at the axis of the column, recorded simultaneously with the heat transfer measurements, are shown in Fig. 7 for $U_g = 6$ m/s. For run A, $T_s(1, 2.35)$ is almost the same as $T_s(0, 2.35)$, while $T_s(1, 3.25) > T_s(0, 3.25)$. This suggests that for these operating conditions, particles in the vicinity of the wall were always ascending, causing the heat transfer from the wall to the suspension to drop continuously from the bottom to the top of the water jacket. However, for all other operating conditions investigated, it appears from the suspension temperature distributions that particles were oscillating both upwards and downwards in the vicinity of the wall, although the fractions of time spent ascending and descending probably differ. As a result, heat transfer is augmented at both ends of the heat exchanger.

4. Modeling heat transfer in HDCFBs

4.1. Particle motion in the vicinity of the wall

As discussed above, except for extremely dilute pneumatic conveying or very dense suspensions, where the particles and gas suspension both travel upwards across the entire cross-section of the riser, the motion of particles in the vicinity of the wall is not uni-directional. Instead, there is intermittent upward motion near the wall interspersed with periods of downward local particle motion. Depending on the superficial gas velocity and the net circulation flux or cross-sectional average suspension density, the net local flux at the wall may be downwards, forming a wall layer corresponding to the fast fluidization flow regime; alternatively the net time-average local flow can be everywhere upward, corresponding to dense suspension upflow.

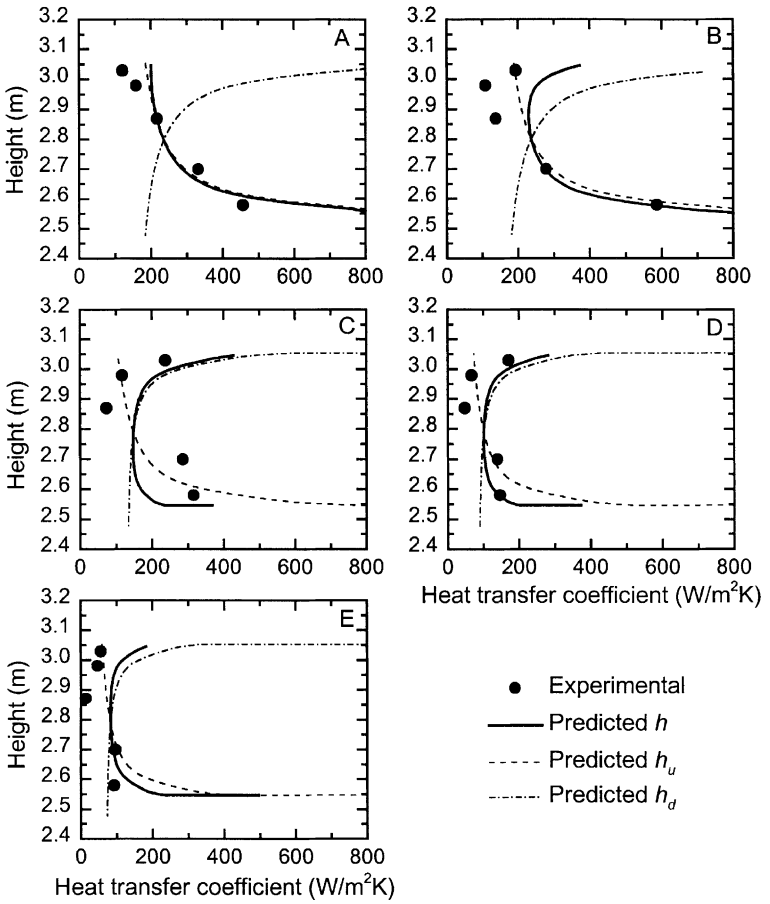

Fig. 5. Comparison of predicted and experimental heat transfer coefficients for $U_g = 6$ m/s. Operating conditions are listed in Table 1.

When particles oscillate upwards and downwards in the vicinity of the wall, the suspension enters the heat transfer section both from below and above. As illustrated in Fig. 8, if particles in the vicinity of wall were all rising, we would expect T_{sbw}, the suspension temperature in the vicinity of wall below the heat exchanger, to equal T_{sbc}, the suspension temperature at the axis of the riser below the heat exchanger. Above the heat exchanger, $T_{stw} > T_{stc}$ since the ascending particles near the wall would gain heat from the walls. Similarly, if the particles in the vicinity of the wall were all descending, we would expect $T_{stw} = T_{stc}$ and $T_{sbw} > T_{sbc}$. If more particles descend than ascend, then $[T_{sbw} - T_{sbc}] > [T_{stw} - T_{stc}]$. In other words, $[T_{sbw} - T_{sbc}]$ is an indicator of the fraction of time that the particles in the vicinity of the wall are descending, while $[T_{stw} - T_{stc}]$ indicates the fraction of time they are rising. Therefore, the fraction of time particles are falling near the wall can be approximated as

$$f_d = \frac{(T_{sbw} - T_{sbc})}{(T_{stw} - T_{stc}) + (T_{sbw} - T_{sbc})}. \quad (7)$$

Fig. 9 shows the time fraction estimated in this manner as a function of the cross-sectional average suspension density for superficial gas velocities of 6 and 8 m/s. The solid lines are quadratic fits to these data. It can be seen that a lower superficial gas velocity favours the downward movement of particles near the wall.

4.2. Extended two-dimensional model for smooth wall

The model developed in Part I assumes that all particles in the wall layer are always descending. As shown above, this is not the case for high-density risers. The model needs to be extended to cover the true situation where particles spend some of the time moving upwards and some descending.

As a first approximation, with the successive periods of upward and downward flow relatively long, two independent flows can be assumed to exist in the vicinity of wall. For part of the time the wall layer is falling from top to bottom; the rest of the time is spent rising. If the

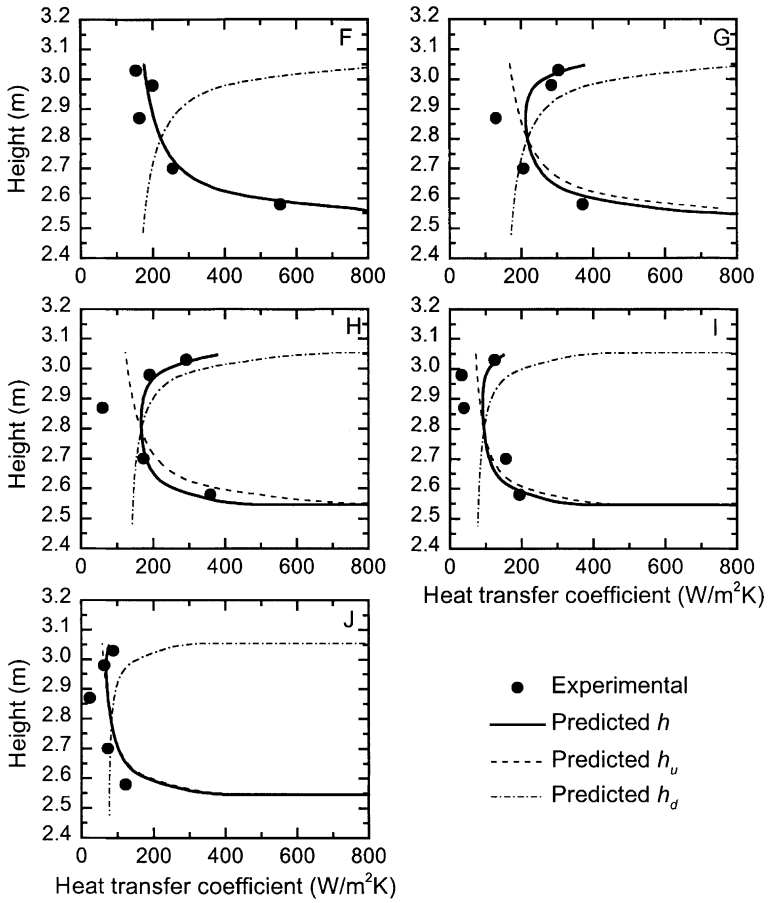

Fig. 6. Comparison of predicted and experimental heat transfer coefficients for $U_g = 8$ m/s. Operating conditions are listed in Table 1.

Table 1
Operating conditions and f_d

Run	A	B	C	D	E
U_g (m/s)	6	6	6	6	6
G_s (kg/m^2 s)	477	372	182	149	51
ρ_{sus} (kg/m^3)	329	335	81	37	24
$T_{stw} - T_{stc}$ (°C)	1.31	1.52	0.87	2.25	4.06
$T_{sbw} - T_{sbc}$ (°C)	0.11	0.46	4.72	6.56	4.86
f_d	0.08	0.23	0.84	0.74	0.54
Run	F	G	H	I	J
U_g (m/s)	8	8	8	8	8
G_s (kg/m^2 s)	527	373	225	135	79
ρ_{sus} (kg/m^3)	262	239	111	34	23
$T_{btw} - T_{btc}$ (°C)	1.05	1.01	0.83	5.68	4.51
$T_{bbw} - T_{bbc}$ (°C)	0	0.43	0.92	2.06	0.43
f_d	0	0.30	0.53	0.27	0.09

heat transfer coefficient due to the former motion h_d, and that due to the latter motion h_u, are calculated from the previous model, then the overall heat transfer coefficient can be obtained by superposition as

$$h = (1 - f_d)h_u + f_d h_d. \quad (8)$$

This approach is a significant oversimplification of a complex, transient problem as it assumes steady fluid

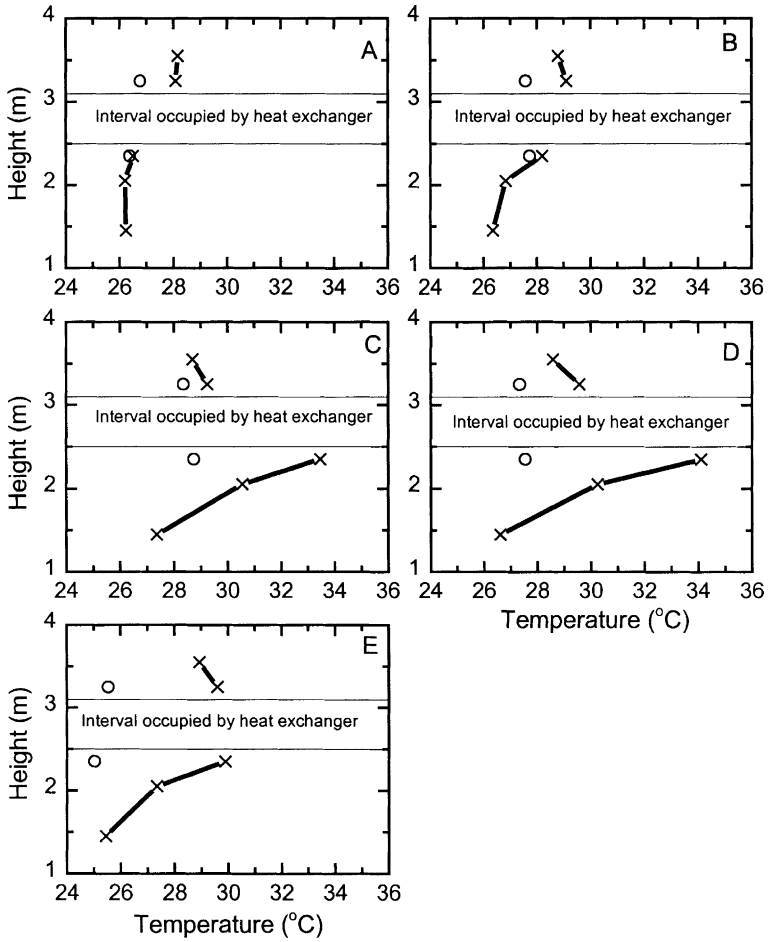

Fig. 7. Suspension temperatures at the wall and axis of the riser for $U_g = 6$ m/s. Operating conditions are listed in Table 1. $\circ : r/R = 0$; $\times : r/R = 1$.

and particle motion during intermittent periods of flow in each direction. Parameters needed to apply the extended model were shown as follows:

1. *Thickness of wall layer:* The correlation of Bi et al. [9], Eq. (24) in Part I, was used to calculate the wall layer thickness in the fast fluidization flow regime. In dense suspension upflow, a distinct wall layer is absent. However, the sensitivity analysis presented below indicates that the layer thickness has negligible influence on the heat transfer coefficient so long as it exceeds the thermal boundary layer thickness. Hence this equation is still employed here, but only when determining the temperature distribution close to the wall.
2. *Particle downward and upward velocities near the wall:* Liu [5] measured the average particle velocity at several elevations in the riser used for the present experiments. His results show that the particle average velocity in the vicinity of the wall is a function not only of such operating conditions as superficial gas velocity and net particle circulation flux, but also of elevation. It is difficult enough to predict the time-average particle velocity in the vicinity of wall, without having to separate it into average upward and downward velocities. For the current study, as a first approximation, 1.2 m/s is employed as the magnitude for both the upward and downward particle velocities.

4.3. Comparison of model predictions with experimental results

Table 1 shows the operating conditions and f_d values calculated from the suspension temperature measurements for superficial gas velocities of 6 and 8 m/s. Local heat transfer coefficients predicted by the model, i.e., Eqs. (7) and (8) with h_d and h_u from Part I, are compared

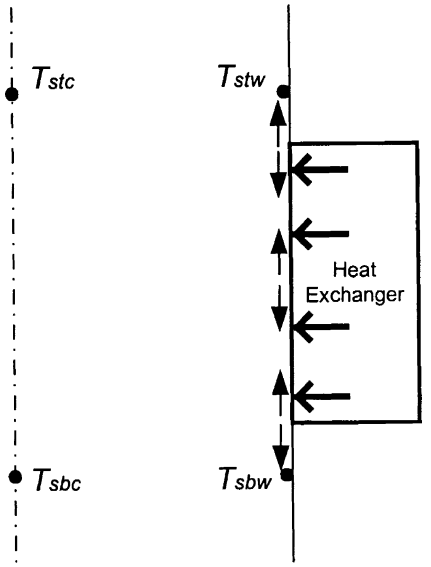

Fig. 8. Schematic of particle motion in the vicinity of the wall and its influence on the suspension temperature.

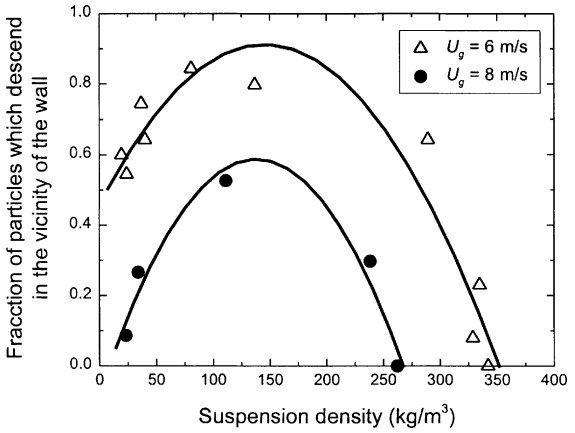

Fig. 9. Fraction of particles moving downwards in the vicinity of the wall as a function of suspension density and superficial gas velocity.

with the experimental data in Figs. 5 and 6 for $U_g = 6$ and 8 m/s, respectively. The dash–dot lines are the heat transfer coefficients (h_d) calculated assuming all particles in the vicinity of the wall to be descending; the dashed lines (h_u) are obtained by assuming all particles are traveling upward. The thick solid lines are the weighted average heat transfer coefficients based on Eqs. (7) and (8). It can be seen that the extended model (with particles oscillating up and down) predictions fit the experimental data quite well, and definitely better than the individual unidirectional (h_d and h_u) predictions.

5. Sensitivity analysis

Part I shows that the two-dimensional model with unidirectional solids motion near the wall gives reasonable predictions for the fast fluidization regime in most cases. By superimposing the heat transfer results when the suspension in the vicinity of wall is allowed to move downwards and upwards separately, the model is also able to predict the trends in our experimental results in high and low density risers. The model presented in Part I is now used to investigate the effect of various parameters on the heat transfer process. Numerous variables play roles in this process. In the sections below, several of the most important and uncertain ones are varied parametrically to observe their influence. In each study, the base case predictions (described in Part I) are indicated by solid lines in the respective diagrams.

5.1. Influence of particle diameter

In this model, the only mechanism by which heat is ultimately transferred to the riser wall is by radiation and by conduction through the gas gap. As shown in Fig. 10(A), the conduction heat flux at the wall increases as the particle diameter decreases, while the radiation flux decreases. The influence of the particle diameter on conduction transfer is greatest near the top of the heat transfer surface. The particle diameter influences the heat transfer process in three ways:

1. Via its influence on the gas gap thickness: The smaller the particles, the thinner the gas gap (since $\delta_g \propto d_p$), and hence the lower the gas gap conduction resistance;
2. Via its influence on heat convection between the gas and particles: Because finer particles have larger total surface areas (for the same voidage), more heat is convected from finer particles to the gas, and then conducted from the gas to the wall;
3. Via its influence on the suspension radiation absorption and scattering: According to Eqs. (21) and (22) of Part I, the suspension absorption and scattering coefficients are proportional to $1/d_p$. Finer particles (at the same voidage) act as a denser curtain between the high temperature core and the wall, thus decreasing the net radiation flux.

Thus, it can be expected that the total heat flux will increase with decreasing particle size at low bed temperatures, where radiation is not significant. At high suspension temperatures, the situation is more complex since the particle diameter affects the convection and radiation heat transfer processes in opposite directions. In this case the heat flux may therefore increase or decrease with decreasing mean particle diameter.

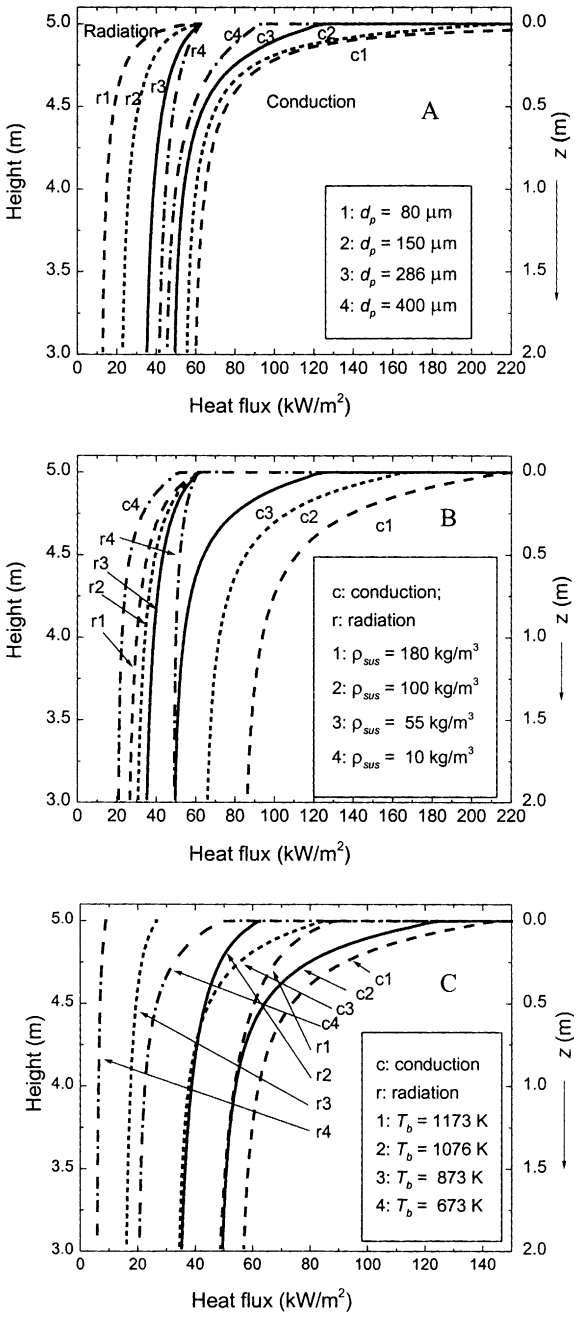

Fig. 10. Influences of physical parameters on vertical heat flux profile. A: particle diameter; B: suspension density; C: bulk temperature. (Base conditions as in Section 4.1 of Part I, except for particle diameter in A, suspension density in B and bulk temperature in C.)

5.2. Influence of suspension density

It is widely recognized that CFB heat transfer is strongly correlated with the overall suspension density. A higher suspension density results in a thicker wall layer having a higher concentration of particles. Also, there is a greater rate of particle exchange between the core and the wall layer which augments the transfer of heat from the bulk to the wall. On the other hand, a thicker wall layer and higher particle concentration increases the radiation resistance between the bulk and wall, thereby decreasing the radiation contribution.

The conduction and radiation heat fluxes calculated for different suspension densities are plotted in Fig. 10(B). The higher the suspension density, the less the relative contribution of radiation, not only because the radiation component is lower, but also because of the increased heat conduction. This predicted influence of suspension density on conduction heat flux is consistent with experimental results (e.g., [8–12]).

5.3. Influence of bulk temperature

Heat flux increases with increasing bulk temperature due to three factors: an increase in radiation, a larger driving force for conduction, and increased thermal conductivity of the gas. Fig. 10(C) shows that the increase in the radiation is higher than the increase in the conduction component for the conditions investigated, consistent with experimental results (e.g., [13–16]).

The influence of some other parameters, such as gas gap thickness, gas velocity, particle physical properties, wall layer thickness, wall-side thermal resistance, water-side heat transfer coefficient, average residence length, etc., were also investigated. Details are given by Xie [3]. Their predicted influences on the heat flux are summarized in Table 2. The upward and downward arrows show the direction of the influence, while the number of arrows roughly indicates the extent of the influence. A dash means that the influence is negligible. All these trends are based on the base operating conditions described in Part I; they might differ if the base conditions were changed significantly.

6. Conclusions and recommendations

Experiments carried out with FCC particles in the 76 mm diameter riser of a dual-loop HDCFB facility show that particles move both upwards and downwards in the vicinity of the wall. The direction of this motion is indicated by the suspension temperature distribution above and below a heat exchange section. Average suspension-to-wall heat transfer coefficients are strongly influenced by suspension density. The local heat transfer coefficient profiles are strongly influenced by the direction of particle motion. Periodic reversal of direction leads to higher heat transfer coefficients at both ends of the heat exchanger.

Table 2
Summary of predicted parameter influences on heat flux for base case conditions listed in Section 4.1 of Part I

Parameter and change direction		Radiative heat flux	Conductive heat flux	Comment
Gas gap thickness	↑	↑	↓↓	
Particle diameter	↑	↑↑↑	↓↓	Higher effect on q_c at top
Suspension density	↑	↓↓	↑↑↑↑↑	
Particle velocity	↑	↑	↑↑	Higher effect at bottom
Gas velocity	↑	↑	↓	
Bulk temperature	↑	↑↑↑↑↑	↑↑↑↑	
Particle emissivity	↑	↑↑	–	
Particle volumetric heat capacity	↑	↑↑	↑↑↑	Smaller effect at top
Particle average residence length	↑	↑↑↑	↑↑↑	Smaller effect at top
Wall layer thickness	↑	–	–	
Wall-side thermal resistance	↑	–	–	
Water-side heat transfer coefficient	↑	–	–	Not significant unless <1000 W/m^2 K

The heat transfer model developed in Part I is extended to cover both high-density and low-density operating conditions considering the actual particle motion in the vicinity of wall by introducing the factor f_d, defined as the fraction of time that particles spend traveling downwards, as estimated from the suspension temperature distribution. The resulting model predictions compare well with the experimental data. The sensitivity of the heat transfer process to changes of various parameters is investigated. The predicted influences of different parameters on the heat flux are also consistent with experimental trends where these are known.

The current model for heat transfer in dense suspension upflow assumes that the steady-state results obtained for two independent layers moving upwards and downwards can simply be superimposed. In reality, particles in the vicinity of the wall alternate between upward and downward motions, yielding an unsteady problem for which the current approach may be insufficient. The model should be further extended to provide a more realistic representation of particle motion near the wall. Heat extraction in CFB combustors is usually accomplished by membrane walls. The current model does not consider the geometry of the membrane walls. It is essential to thoroughly understand the mechanisms of heat transfer between the gas-solid suspension and the membrane wall surface, to consider the heat conduction in membrane walls, and to develop an appropriate model to predict the rate of heat transfer.

Suspension-to-wall heat transfer is strongly influenced by the system hydrodynamics, especially the particle and gas motion in the vicinity of the wall. However, hydrodynamic studies on high-density circulating fluidized beds are limited. Both experimental and modeling studies are needed to extend understanding of particle and gas motion in high-density flow regimes.

Acknowledgements

Financial support from the Natural Sciences and Engineering Research Council of Canada is gratefully acknowledged.

References

[1] J.X. Zhu, H.T. Bi, Distinctions between low density and high density circulating fluidized beds, Can. J. Chem. Eng. 73 (1995) 644–649.
[2] J.R. Grace, A.S. Issangya, D. Bai, H.T. Bi, Situating the high-density circulating fluidized bed, AIChE J. 45 (1999) 2108–2116.
[3] D. Xie, Modeling of heat transfer in circulating fluidized beds, Ph.D. Thesis, University of British Columbia, Vancouver, Canada, 2001.
[4] A.S. Issangya, Flow dynamics in high density circulating fluidized beds, Ph.D. Thesis, University of British Columbia, Vancouver, Canada, 1998.
[5] J. Liu, Particle and gas dynamics of high density circulating fluidized beds, Ph.D. Thesis, University of British Columbia, Vancouver, Canada, 2001.
[6] R.L. Wu, C.J. Lim, J. Chaouki, J.R. Grace, Heat transfer from a circulating fluidized bed to membrane waterwall surfaces, AIChE J. 33 (1987) 1888–1893.
[7] J.C.L. Furchi, L. Goldstein, G. Lombardi, M. Mohseni, Experimental local heat transfer in a circulating fluidized bed, in: P. Basu, J.F. Large (Eds.), Circulating Fluidized Bed Technology II, Pergamon, 1988, pp. 263–270.

[8] R.J. Divilio, T.J. Boyd, Practical implications of the effect of solids suspension density on heat transfer in large scale CFB boilers, in: A.A. Avidan (Ed.), Circulating Fluidized Bed Technology IV, AIChE, New York, 1994, pp. 334–339.
[9] H.T. Bi, J. Zhou, S-Z. Qin, J.R. Grace, Annular wall layer thickness in circulating fluidized bed risers, Can. J. Chem. Eng. 74 (1996) 811–814.
[10] J.R. Grace, Heat transfer in circulating fluidized beds, in: P. Basu (Ed.), Circulating Fluidized Bed Technology, Pergamon, 1986, pp. 63–81.
[11] L.R. Glicksman, Circulating fluidized bed heat transfer, in: P. Basu, J.F. Large (Eds.), Circulating Fluidized Bed Technology II, Pergamon, New York, 1988, pp. 13–29.
[12] C. Werdermann, J. Werther, Heat transfer in large-scale circulating fluidized bed combustors of different sizes, in: A.A. Avidan (Ed.), Circulating Fluidized Bed Technology IV, AIChE, New York, 1994, pp. 428–435.
[13] H. Kobro, C. Brereton, Control and fuel flexibility of circulating fluidized beds, in: P. Basu (Ed.), Circulating Fluidized Bed Technology, Pergamon, 1986, pp. 263–272.
[14] B.A. Andersson, F. Johnsson, B. Leckner, Heat transfer measurements in fluidized bed boilers, in: J.P. Mustonen (Ed.), Proceedings of 9th International Fluidized Bed Combustion Conference, vol. 1, ASME, New York, 1987, pp. 592–598.
[15] B.A. Andersson, B. Leckner, Experimental methods of estimating heat transfer in circulating fluidized bed boilers, Int. J. Heat Mass Transfer 35 (1992) 3353–3362.
[16] R.L. Wu, J.R. Grace, C.J. Lim, C.M.H. Brereton, Suspension-to-surface heat transfer in a circulating fluidized bed combustor, AIChE J. 35 (1989) 1685–1691.